Wiley Online Library
Early View publication on www.wileyonlinelibrary.com
(issue and page numbers not yet assigned;
citable using Digital Object Identifier – **DOI**)

Laser Photonics Rev., 1600115 (2017) / **DOI** 10.1002/lpor.201600115

LASER & PHOTONICS REVIEWS

Abstract Femtosecond laser machining has been widely used for fabricating arbitrary 2.5 dimensional (2.5D) structures. However, it suffers from the problems of low fabrication efficiency and high surface roughness when processing hard materials. To solve these problems, we propose a dry-etching-assisted femtosecond laser machining (DE-FsLM) approach in this paper. The fabrication efficiency could be significantly improved for the formation of complicated 2.5D structures, as the power required for the laser modification of materials is lower than that required for laser ablation. Furthermore, the surface roughness defined by the root-mean-square improved by an order of magnitude because of the flat interfaces of laser-modified regions and untreated areas as well as accurate control during the dry-etching process. As the dry-etching system is compatible with the IC fabrication process, the DE-FsLM technology shows great potential for application in the device integration processing industry.

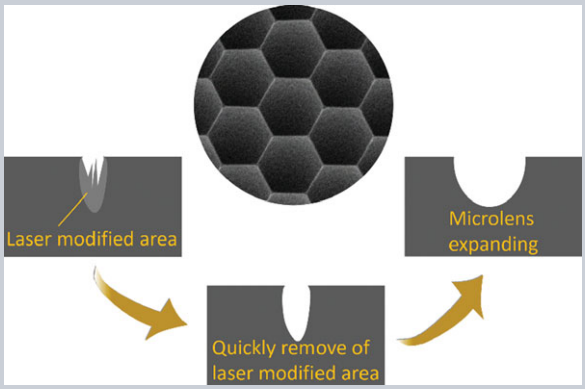

ORIGINAL PAPER

Dry-etching-assisted femtosecond laser machining

Xue-Qing Liu[1], Qi-Dai Chen[1,*], Kai-Min Guan[1], Zhuo-Chen Ma[1], Yan-Hao Yu[1], Qian-Kun Li[1], Zhen-Nan Tian[1], and Hong-Bo Sun[1,2,*]

1. Introduction

Owing to its advantages in constructing arbitrary three-dimensional (3D) structures with high resolution [1, 2], femtosecond laser direct writing (FsLDW) has been widely used for fabricating devices that exhibit broad potential applications in micro-optics [3] and microelectronics [4]. Not only functional photonic crystals [5] and conductive 3D structures [6] could be flexibly fabricated by two-photon- or multiphoton-induced polymerization [7, 8], but also periodic surface structures [9] and waveguides [10] could be optionally manufactured via femtosecond laser machining (FsLM). As one type of FsLDW technology, femtosecond laser ablation is an efficient method for processing hard materials. Normally, as a point-by-point processing method, this FsLM technology suffers from the problem of low fabrication efficiency: it is time consuming to fabricate large-volume structures, even in the case of structures with dimensions of the order of millimeters. Furthermore, a high laser power is necessary for complete materials ablation when processing hard materials, leading to a high surface roughness that is much worse than that required for the suitable optical quality [11]. An effective strategy for eliminating the damage to materials is the reduction of laser power to activate the irradiated regions without the removal of materials. After femtosecond laser irradiation with low power, the material properties (chemical composition and chemical energy) of the irradiated area would be changed [12, 13]. The smoothness of the interface of laser modified and untreated areas at low laser power is better than that of the surface after high laser power ablation. Therefore, well-defined structures with smooth surfaces could be flexibly fabricated by femtosecond laser modification with etching. As the chemical component and chemical energy of the irradiated area would be changed after the femtosecond laser modification with low power, the etching rate is different between the laser-treated and untreated regions [14]. Nowadays, chemical wet etching is used to remove laser-modified regions for fabricating microchannels in transparent materials and microlens on silicon [15, 16]. In most cases, chemical wet etching is isotropic (except for the difference of crystal-orientation-based etching), thus making it easy to form 3D microstructures via combination of femtosecond laser and chemical wet etching [17, 18]. However, the distortion of designed structures would result in its incompatibility with the integrated circuit (IC) fabrication process, which was caused by serious lateral etching of chemical wet etching when transferring lithography patterns to the substrate materials. Thus, it limits the potential application of FsLM followed by the chemical wet-etching process in device integration.

Dry-etching technology was developed to address the need of integrated circuit technology, and it has been developed along with the continuous micronization and high integration of integrated circuits. As it has high precision, which can be flexibly controlled, dry-etching technology has also

[1] State Key Laboratory on Integrated Optoelectronics College of Electronic Science and Engineering Jilin University, 2699 Qianjin Street, Changchun, 130012, P.R. China
[2] College of Physics, Jilin University, 119 Jiefang Road, Changchun, 130023, P.R. China
*Corresponding Authors E-mail Address: chenqd@jlu.edu.cn, hbsun@jlu.edu.cn

been widely used in the fabrication of plasmonics and metamaterials [19], optical nanocavities [20], optomechanical circuits [21], memory devices [22], and solar cells [23]. In this paper, to overcome the disadvantages of the conventional FsLM approach, we propose a dry-etching-assisted femtosecond laser machining (DE-FsLM) approach for the first time. This process consists of the construction of microholes through the femtosecond laser modification of various materials, following which the laser-irradiated regions are removed by dry etching. As the power required for the laser modification of materials is lower than that required for laser ablation, the process efficiency would be increased for the formation of complicated 2.5-dimensional (2.5D) structures. Notably, high-precision structures could be fabricated owing to the flat interfaces between laser-modified regions and untreated areas as well as accurate control during the dry-etching process.

2. Experimental section

Materials and laser fabrication: The surfaces of undoped <100>-oriented silicon wafers were ultrasonically cleaned in acetone, ethanol, and deionized water. Laser exposure was performed using an amplified Ti: sapphire femtosecond laser system (Spectra Physics) that delivers 100 fs pulses having a 800-nm central wavelength with a repetition rate of 1 kHz. The laser beam was focused by an objective lens with a numerical aperture (NA) of 0.8 at normal incidence to the surface of the silicon wafer. After laser irradiation, the silicon samples were ultrasonically cleaned in acetone, ethanol, and deionized water.

Dry-etching process: All samples were etched using an induction coupling plasma (ICP, ULVAC CE 300I) instrument. The ICP processing conditions were 1 Pa APC pressure, 5 Pa trigger pressure, 5 Pa PFC pressure, 400 W antenna RF power, and 40 W bias RF power. The etching time was adjusted for fabricating different structures.

Surface characterization: Field-emission scanning electron microscopy (FE-SEM, JEOL JSM-6700F, Japan) and laser scanning confocal microscopy (LSCM, OLS4100, Japan) were utilized to measure the surface morphologies of the samples. The surface roughnesses of samples were measured by atomic force microscopy (AFM, Dimension Icon, Bruker Corporation).

3. Results and discussion

3.1. Principle of DE-FsLM fabrication

Figure 1 illustrates the route for fabricating microstructures with femtosecond laser modification followed by the dry-etching process. It is well known that silicon is one of the most important materials in the IC industry. Therefore, its ability to be applied for manufacturing silicon functional architectures is an important factor to evaluate the performance of a new fabrication technology. Thus, we chose silicon for evaluating the ability of DE-FsLM. As an example, silicon concave microlenses were fabricated by this method. First, an 800-nm linearly polarized femtosecond laser beam with a width of 100 fs and repetition rate of 1 kHz was focused by an objective lens with numerical aperture (NA) of 0.8 on the surface of the silicon wafer. After the femtosecond laser modification, a microhole array could be formed on the surface of the silicon wafer. Subsequently, the silicon samples were etched in SF_6 plasma gas through induction coupling plasma for fabricating the designed structures. The reason for choosing ICP as the equipment for dry etching was its facile adjustment for vertical and lateral etching. The antenna RF power and bias RF power were 400 W and 30 W, respectively, and the gas flux of SF_6 was 40 sccm. The diameters of the concave structures increased with etching time, rendering the formation of concave microlenses, as shown in Fig. 1a. Figure 1b illustrates the variation tendency of the diameter and depth of concave structures with etching time. The etching process has two stages: primarily, the laser-modified region is quickly etched during the initial etching stage, and subsequently, the concave structures expanded along with etching time in the stable etching stage.

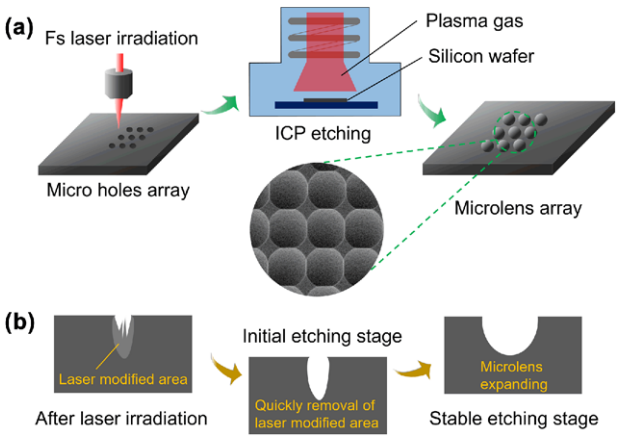

Figure 1 (a) Schematic diagram of the fabrication of silicon structures using DE-FsLM. The inset shows the SEM image of the fabricated silicon concave structures. (b) Schematic diagram of the cross-sectional profiles of the concave structures to illustrate the etching process.

Figure 2a shows the experiment results concerning the variation tendency of the diameter and depth of concave structures with etching time. The femtosecond laser power is 300 nJ/cm^2, and the pulse number is 50 for fabricating the concave structures. According to Fig. 2a, the diameters of the concave structures increased almost linearly with the etching time, suggesting that the lateral etching rate is stable with increasing etching time. However, the depth of the concave structures rapidly increased to a maximum value after the initial several minutes of etching, demonstrating that the laser-modified region could be quickly etched during the initial procedure. The etching rate of the laser-modified region is about 4 times larger than that of unmodified silicon, as shown in Fig. S1. Under the same conditions, the etching rate of laser-modified region is about 4 μm/min, while the

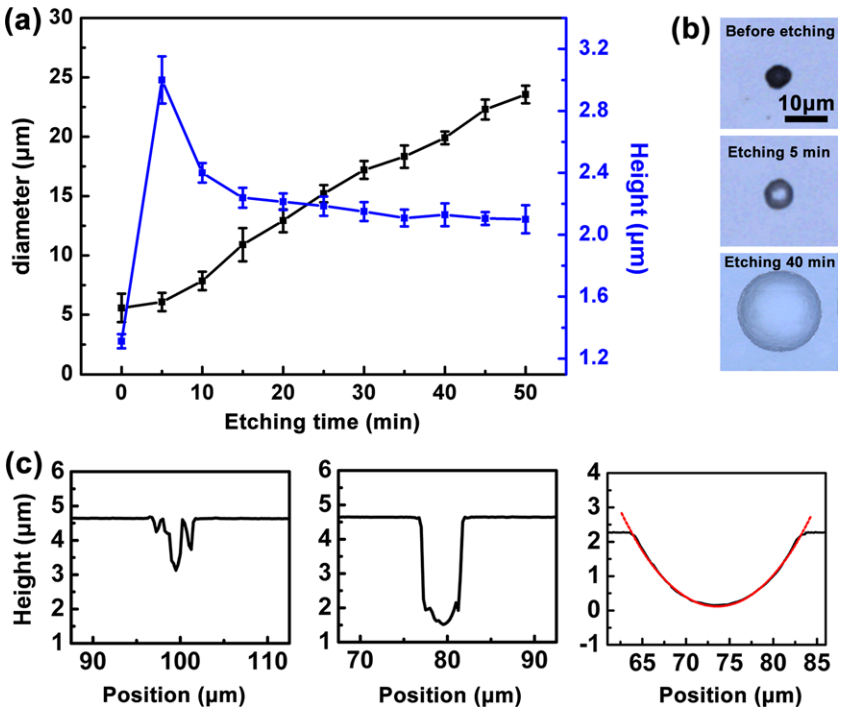

Figure 2 (a) Dependence of diameter and depth of silicon concave structures on etching time. (b) Optical image of microstructures formed after laser irradiation, with etching for 5 min and 40 min. (c) Cross section of the concave structures corresponding to (b). The red line in (c) is the fitted curve of concave structures after etching for 40 min.

etching rate of unmodified silicon is about 1 μm/min. In the initial procedure, the laser-modified region was quickly removed and the concave structures became smooth with increasing etching time. After laser irradiation, the crystal silicon would absorb the energy of laser pulses, resulting in the damage of some of the silicon atoms bonding and also excitation of some others. So in this way, crystal silicon would be transformed to polycrystalline silicon [24]. In the dry-etching process, it was easier for the bond rupture of polycrystalline silicon. Thus, the etching rate of the laser-modified region is larger than that of unmodified silicon. After several minutes of etching, the depth of the concave structures slowly decreased and tended to be constant with further increase in etching time, which seems extraordinary. In fact, aspect ratio dependent etching (ARDE), which is also called the aperture effect, could cause an insufficient supply of local gas, thereby giving rise to the decrease of etching rate at the bottom of concave structures [25]. More clearly, the etching process is affected by the amount of etching gas on the sample surface. It is challenging for the gas to reach the bottom of the concave structure, and so was the reaction product to be exhausted from the bottom. Therefore, the dry etching rate in the vertical direction for silicon outside the concave structure was greater than that inside the concave structure, which caused the depth of the concave structure to decrease after etching for a few minutes. However, when the aspect ratio of concave structures is no more than 0.5 as shown in Fig. 2a, the aperture effect is weakened with further increase in etching time. Hence, the variation in depth of concave structures is negligible in the stable etching stage. Optical microscope images in Fig. 2b show the concave structures fabricated after femtosecond laser irradiation, followed by ICP etching for 5 min and 40 min, respectively. As etching proceeds, the top morphology of concave structures changed from an irregular circle to a regular circle. A high-resolution SEM image of the crater is shown in Fig. S2, which is fabricated by the fs laser irradiation under laser power of 300 nJ/cm^2 and pulse number of 50. This indicated that after laser irradiation, an irregular circle with scattered particles is formed on the surface of silicon, while after etching, a regular circle could be formed. Figure 2c shows the cross-sectional profile of the concave structures after femtosecond laser modification and etching for 5 min and 40 min, respectively. From the above, it could be concluded that modified regions were formed after the laser irradiation, and the dry-etching rate of modified regions was higher than that of untreated regions. After the etching of modified regions for a few minutes, the concave structures expanded with increasing etching time. In Fig. 2c, the red line represents the profile of a theoretical sphere model (R = 23.35 μm), which fits the solid line representing the measured profile of the concave structures. The residual sum of squares (RSS) between the actual and ideal profiles was 0.157 with a root-mean-square error (RMSE) of approximately 31.8 nm, indicating that microconcave structures have excellent spherical profiles.

Surface smoothness is crucial for microstructures applied in optical devices. Therefore, surface roughness defined by the root-mean-square (RMS) of a polished silicon wafer, a polished silicon wafer after etching for 20 min, a laser-structured silicon surface and microlens fabricated by DE-FsLM were measured by atomic force microscopy (AFM), as shown in Fig. S3. The surface roughness are 0.3, 5.6, 175 and 8 nm, respectively. The surface roughness of a polished silicon wafer would be slightly increased to several nanometers after dry etching, which is caused by the

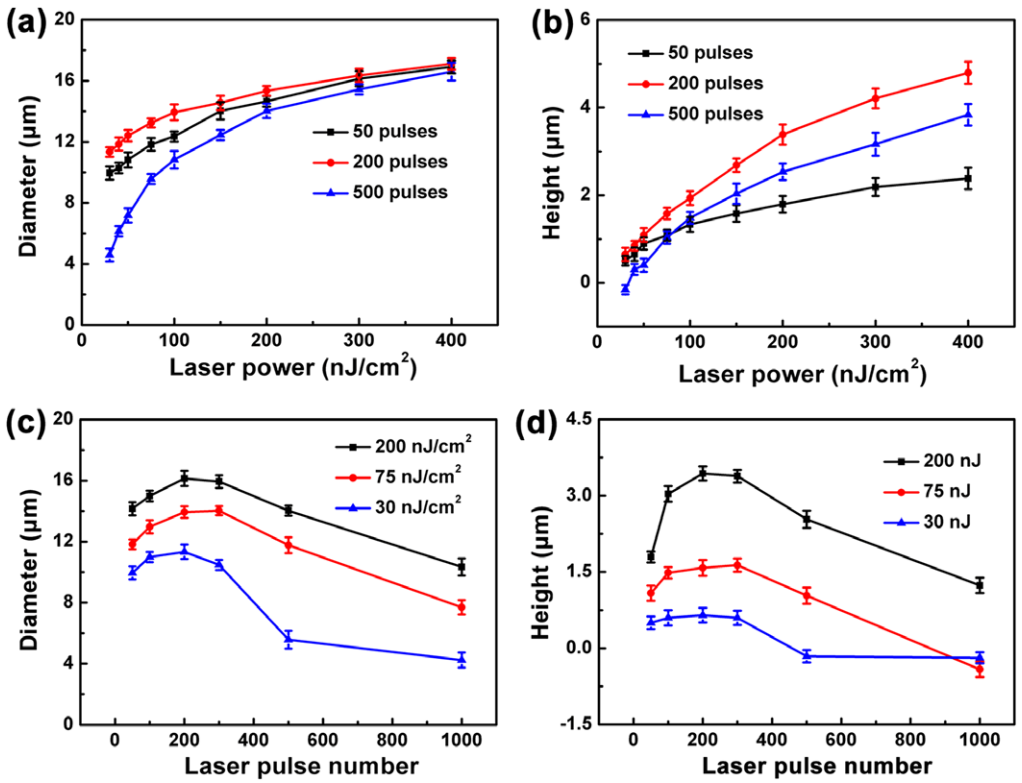

Figure 3 Dependence of diameter (a) and height (b) of the concave structures on laser power. The pulse numbers are 50, 200, and 500, respectively. (c) and (d) show the dependence of the diameter and height of the concave structures on the number of pulses. The pulse powers are 30 nJ/cm^2, 75 nJ/cm^2, and 200 nJ/cm^2.

bombardment of SF_6 plasma on the substrate. The surface roughness of the laser-structured silicon wafer is increased to a value that is three orders of magnitude lager than that of polished silicon wafer, which is much worse than that required for the suitable optical quality. The large surface roughness of laser-structured silicon wafer is mainly caused by scattering particles and depth undulation that formed during laser processing. Notably, compared with a laser-structured wafer, the surface roughness of a microlens fabricated by DE-FsLM is decreased to several nanometers, which is almost the same as polished silicon after etching. It could be concluded that surface roughness of a laser-structured wafer could be improved via a dry-etching process.

3.2. Adjustment of microlens profiles

As the microconcave structures have good spherical profiles, concave spherical microlenses could be successfully fabricated by DE-FsLM. The focal length could be adjusted by changing the diameter and height of the concave structure. The femtosecond laser power has an effect on the area of the modified region. Thus, the diameter and depth of the structures formed after dry etching could be adjusted by changing the laser power. To investigate the dependence of the size of concave structures on the laser power, three groups of different numbers of laser pulses are irradiated on the silicon surface with different laser powers. The numbers of laser pulses are 50, 200, and 500, and the laser power is controlled in the range of 20 nJ/cm^2 to 150 nJ/cm^2. Then, all the samples are etched for 30 min using SF_6 with ICP. Figures 3a and b show the diameter and depth of the concave structures at different laser powers, respectively. It could be concluded that the diameter and depth of the concave structures increased with increasing laser power. The accumulation of laser pulses also has the ability to influence the size of modified regions. The laser powers are 30 nJ/cm^2, 75 nJ/cm^2, and 200 nJ/cm^2, the range of the numbers of laser pulses is controlled from 50 to 500, and the etching time is 30 min. Figures 3c and d exhibit the relationship between the diameter or depth of the concave structures and the number of laser pulses, respectively. The results demonstrate that diameter and depth of the concave structures increased to a maximum value on increasing the number of laser pulses and then decreased if the number of laser pulse number was further increased. Figure S4a shows optical microscope observations of the microstructure fabricated at a laser power of 30 nJ/cm^2, with an etching time of 30 min, and the pulse numbers of 50, 100, 200, 300, 500, and 1000. The convex cone structure could even be formed with a pulse number of 1000, as shown in Fig. S4b. It has been proved that oxygen could be incorporated and the crystal structure could be changed

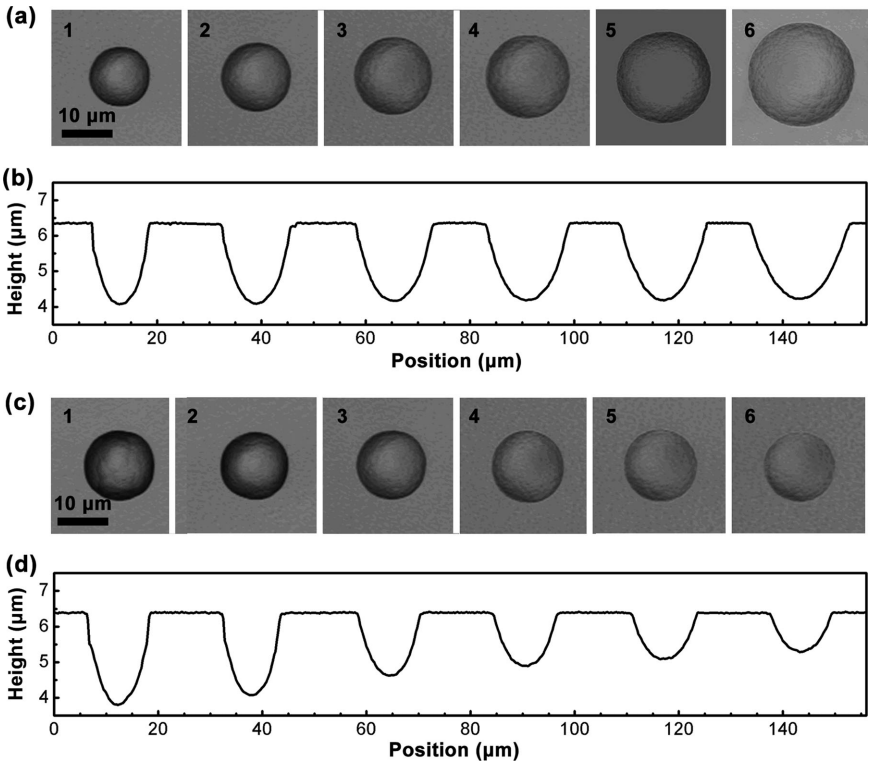

Figure 4 (a) Optical images and (b) cross section of the concave microlens with different diameters and same height fabricated using DE-FsLM. (c) Optical images and (d) cross section of the concave microlens with different heights and same diameter fabricated by adjusting the laser power and etching time. All the optical images and cross-sectional lines are obtained using laser scanning confocal microscopy (LSCM).

from crystalline to amorphous in the modified regions after laser irradiation [26]. Along with the increase in the size of modified regions, the amount of oxygen increased with increasing pulse number, as shown in Fig. S5. The etching rate of silicon is greater than that of silicon oxides when etched by SF_6, thus resulting in a competition between the rapid etching of amorphous silicon in the modified region and the inhibiting effect of etching oxide silicon in the etching process. The rapid etching of amorphous silicon plays a dominant role when the number of laser pulses was less than approximately 200, whereas the passivation effect of etching oxide silicon begins to dominate when the number of laser pulses is greater than approximately 200. From the above, it is obvious that the morphology of microstructures could be flexibly adjusted by controlling the activation and passivation effect.

According to Figs. 2 and 3, the diameter and height of the concave microlens could be individually controlled by adjusting femtosecond laser power, pulse number, and etching time. The photographs in Fig. 4a show the concave microlens with different diameters and identical height fabricated by DE-FsLM. The femtosecond laser power is 200 nJ/cm^2 for fabricating all the microlenses, and the etching time is increased from 15 min to 40 min with an interval of 5 min, corresponding to photoimages "1" to "6" in Fig. 4a. The cross-sectional profiles of concave microlenses are shown in Fig. 4b, and they indicate that concave microlenses possessing an identical height with varying diameters could be fabricated using the same laser power with different etching time. Furthermore, microlenses with the same diameter and varying height could be realized by adjusting the laser power and etching time, as shown in Figs. 4c and d. The femtosecond laser power is 400, 300, 200, 150, 100, and 50 nJ/cm^2, and the etching time is 15, 17.5, 20, 22.5, 30, and 35 min, corresponding to photoimages "1" to "6" in Fig. 4c. The cross-sectional profiles of concave microlenses are shown in Fig. 4d, indicating that concave microlenses with a similar diameter and different heights could be fabricated by adjusting the laser power with different etching time. It could be concluded that the height of the concave microlens is determined by the laser power and the diameter could be adjusted by the etching time, which further indicated that the height and diameter of the concave microlens could be predesigned by selecting the appropriate laser power and etching time. From the above, microlenses with diameters of 4 μm to 24 μm and depths of 0.4 μm to 3.4 μm could be fabricated by DE-FsLM under the existing conditions.

3.3. Fabrication of a microlens array and characterization of its imaging property

As discussed above, after ICP etching, concave structures could be expanded to a relatively smooth, curved surface, which could function as a concave microlens. Here, we fabricated an all-silicon uniform-close-packed honeycomb concave microlens array through DE-FsLM, which has potential applications in infrared devices. The fill factor of the microlens array could reach as large as approximately 100%. The top view of the microlens array obtained using a scanning electron microscope (SEM) is shown in Fig. 5a. The laser power used for fabricating these microlenses was 300 nJ/cm^2, and the etching time was 60 min. The distance

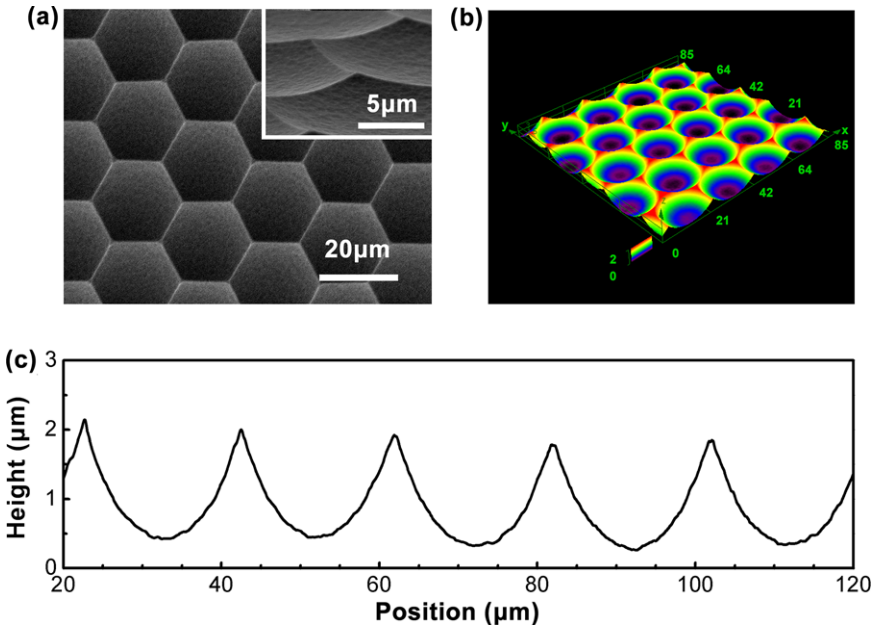

Figure 5 (a) SEM images of all-silicon uniform-close-packed honeycomb concave microlens array fabricated using DE-FsLM. The inset of (a) is the 60°-titled image of the structures. (b) and (c) are the 3D and cross-sectional profiles obtained using LSCM, respectively.

between two adjacent microlenses is 20 μm. The concave microlenses have smooth, curved surfaces, and no wrinkles were formed as the overlap of two pulses formed modified regions, as shown in the inset image of Fig. 5a. The 3D and cross-sectional profiles of the concave microlens array, which were obtained using LSCM, are shown in Figs. 5b and c, respectively. The microlens height is approximately 1.6 μm, which is less than that of the microlens at the edge of the array (the height of which is approximately 2.15 μm, as shown in Fig. S6) fabricated under the same conditions. The discrepancy in height originates from the overlap of two adjacent microlenses. As the concave microlenses have spherical surfaces, the optical parameters of the concave microlenses conform to geometrical optics. For the reflection imaging mode, the radius of curvature (R), focal length (f), image distance (s'), and lateral magnification (V) are estimated using the following equations:

$$R = \frac{h^2 + r^2}{2h}, f = -\frac{R}{2}, \frac{1}{s'} + \frac{1}{s} = -\frac{2}{R}, V = -\frac{s'}{s}, \quad (1)$$

where h is the height of the microlens, r is the radius of the microlens, and s is the object distance (here, s = 170 μm). By using Eq. (1), the radius of curvature, focal length, image distance, and lateral magnification are calculated as 49.6 μm, 24.8 μm, 29.2 μm, and 0.172, respectively. As the arrangement mode could be flexibly adjusted by patterning the microhole array formed by laser irradiation, not only could the close-packed honeycomb concave microlens array but also a close-packed aligned concave microlens array could be fabricated on silicon wafers (as shown in Fig. S7).

The reflected imaging system is adopted for characterizing the imaging property of the concave microlens, which is shown in Fig. 6a. The letter "A" is written by FsLM on a glass slide with a thickness of 170 μm. Subsequently, the glass slide is placed between the objective lens of an optical microscope and the silicon concave microlens array. The images of the letter "A" array can be clearly observed using a charge coupled device (CCD) camera, as shown in Fig. 5b. The lateral magnification of the concave microlens is measured as 0.17, which agrees well with the theoretical value. As one type of microlens, silicon concave microlenses have wide application in infrared optical scanner [27] and combined lens for optical systems. Also, as one type of concave structure, the silicon concave microstructures may be applied in free-space light coupling [28], optical tweezers [29] and increasing light extraction efficiency of silicon based light-emitting diode arrays similar to PDMS concave microstructures for InGaN LEDs [30]. In addition, the silicon concave microlens could also be used as molds for duplicating of polymer convex microlens, as shown in Fig. S8. The transferred PDMS convex microlens arrays show a clear imaging property.

3.4. Integration of DE-FsLM with IC technology

Nowadays, the compatibility of combining femtosecond laser direct writing approach and a photolithographic one on the same sample has attracted more and more concern. It also becomes an important factor that whether the direct writing method can be used in IC industry. In order to investigate the compatibility of DE-FsLM and IC technologies, two types of methods are proposed in this section. First, microstructures could be fabricated on the pre-existing devices. Microstructures could be exactly fabricated at the designated position on the substrates by femtosecond laser direct writing technology. Figure 7a shows a single silicon cantilever, which is a crucial device in microelectromechanical systems (MEMS). It was

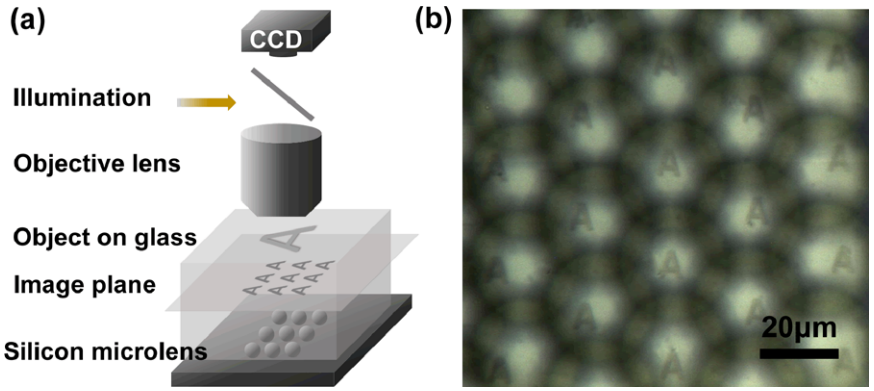

Figure 6 (a) Schematic of the reflection imaging system adopted for characterizing the imaging property of the concave microlens. (b) Optical photograph of the "A" patterns, formed by the concave microlens arrays, visualized using a CCD camera.

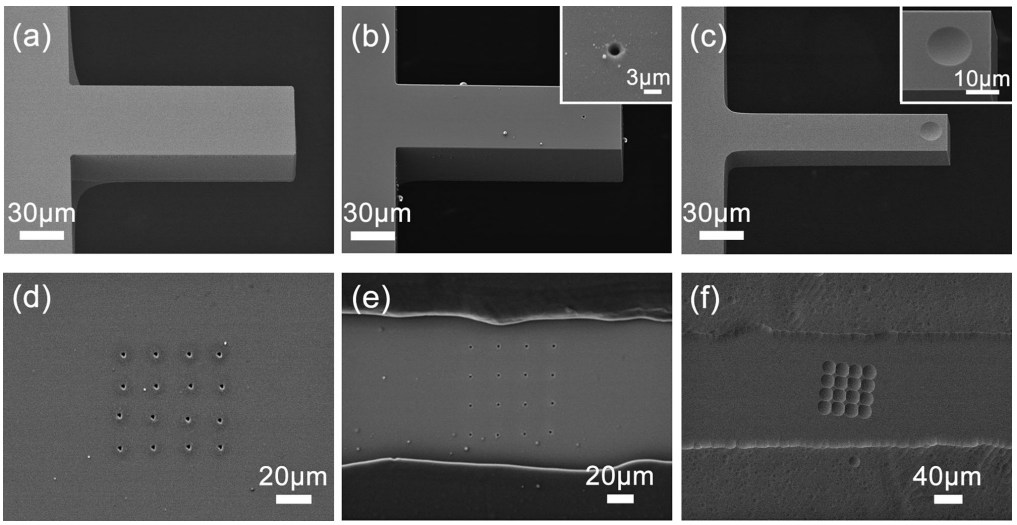

Figure 7 SEM images of microcantilever before laser irradiation (a), microcantilever with a microhole fabricated by FsLM (b) and microcantilever with a microlens fabricated by DE-FsLM (c), respectively. Insert images in (b) and (c) are amplified images. (d) Microhole arrays fabricated on silicon wafer, (e) photoresist pattern fabricated on laser-structured silicon wafer, (f) concave microlens on the bottom of silicon microchannel formed after dry etching.

fabricated on a 4-inch silicon wafer by photolithography IC technology, as shown in Fig. S9. Then, a microhole was exactly fabricated at the designated position on the cantilever, as shown in Fig. 7b. After dry etching of 20 min, a concave microlens could be formed on the silicon cantilever (Fig. 7c). The integration of a microlens on a silicon cantilever may have potential application in micro-optical electronic mechanical systems (MOEMS). Except for integrating microstructures on pre-existing devices, the femtosecond laser direct writing approach could also be integrated into the lithography process. For example, silicon concave microlens arrays could be formed with the fabrication of microchannels. First, microholes arrays were fabricated on a polished silicon wafer by femtosecond laser direct writing (Fig. 7d). Then, photoresist patterns could be formed on the wafer after aligned lithography and developing (Fig. 7e). Finally, silicon concave microlens arrays could be fabricated on the bottom of the silicon microchannel (Fig. 7f). Therefore, this indicated that the combination of laser direct writing and photolithography could be realized on the same sample. Except for microlenses, continuous lines and 2D patterns also can be fabricated by DE-FsM technology, as shown in Figs. S10 and S11. Thus, more complex microstructures can be realized by the method that combines photolithography and DE-FsM.

4. Conclusions and outlook

In summary, DE-FsLM micronanofabrication technology is proposed for the first time. In the DE-FsLM approach, modified regions are formed after laser irradiation. The chemical composition and chemical energy could be changed, resulting in the difference of the dry-etching rate between modified regions and untreated regions. The diameter and height of the structures formed after dry etching could be adjusted by changing the laser power, pulse number, and etching time. Through proper adjustment of the laser power, etching time, and arrangement of exposure spots, an all-silicon uniform-aligned concave microlens array was fabricated by DE-FsLDW. The silicon microlens arrays are considered to have high potential for application in infrared devices, such

as an infrared scanner that is widely used in MOEMS. In addition, other complicated silicon structures could be explored in the future. Although we fabricated only silicon structures with this method in the present work, we believe that various materials could be used to fabricate flexible structures by changing the etching gas, in particular some hard-to-process materials, such as diamond and sapphire. Also, the dry-etching system is unlimited on ICP equipment. As the proposed dry-etching system is compatible with the IC fabrication process, the combination of femtosecond laser machining and photolithography could be realized on the same sample. Thus, the DE-FsLM technology holds great potential for application in the device integration processing industry.

Supporting Information

Additional supporting information may be found in the online version of this article at the publisher's website.

Acknowledgements. Thanks go to the Shanghai Institute of Microsystem and Information Technology, CAS for the fabrication of microcantilevers. The authors acknowledge the supports from National Science Foundation of China (NSFC) and National Basic Research Program of China (973 program) under Grants #51335008, #91423102, #91323301, #61590930, and #2014CB921302.

Received: 8 May 2016, **Revised:** 22 February 2017,
Accepted: 28 February 2017

Published online: 29 March 2017

Key words: femtosecond laser, dry etching, silicon, concave microlens, micronanofabrication.

References

[1] C.N. LaFratta, J.T. Fourkas, T. Baldacchini, R.A. Farrer, Angew. Chem. Int. Ed. **46**, 6238–6258 (2007).
[2] K.-S. Lee, R. H. Kim, D.-Y. Yang, S.H. Park, Prog. Polym. Sci. **33**, 631–681 (2008).
[3] M.D. Turner, M. Saba, Q. Zhang, B.P. Cumming, G.E. Schroder-Turk, M. Gu, Nature Photon. **7**, 801–805 (2013).
[4] Y. Son, J. Yeo, H. Moon, T.W. Lim, S. Hong, K.H. Nam, S. Yoo, C.P. Grigoropoulos, D.-Y. Yang, S.H. Ko, Adv. Mater. **23**, 3176–3181 (2011).
[5] B. Oktem, I. Pavlov, S. Ilday, H. Kalaycioglu, A. Rybak, S. Yavas, M. Erdogan, F.O. Ilday, Nature Photon. **7**, 897–901 (2013).
[6] K. Sugioka, Y. Cheng, Light Sci. Appl. **3**, e149 (2014).
[7] J. Stampfl, R. Liska, A. Ovsianikov, Multiphoton Lithography: Techniques, Materials, and Applications, (Wiley, Hoboken, NJ, USA, 2016).
[8] T. Baldacchini, Three–Dimensional Microfabrication Using Two-Photon Polymerization: Fundamentals, Technology and Applications, (William Andrew, Oxford, UK, 2016).
[9] K.K. Seet, V. Mizeikis, S. Matsuo, S. Juodkazis, H. Misawa, Adv. Mater. **17**, 541–545 (2005).
[10] E. Blasco, J. Müller, P. Müller, V. Trouillet, M. Schön, T. Scherer, C. Barner-Kowollik, M. Wegener, Adv. Mater. **28**, 3592–3595 (2016).
[11] B.N. Chichkov, C. Momma, S. Nolte, F.v. Alvensleben, A. Tünnermann, Appl. Phys. A **63**, 109–115 (1996).
[12] A. Vailionis, E.G. Gamaly, V. Mizeikis, W. Yang, A.V. Rode, S. Juodkazis, Nature Commun. **2**, 445 (2011).
[13] R.R. Gattass E. Mazur, Nature Photon. **2**, 219–225 (2008).
[14] S. He, F. Chen, K. Liu, Q. Yang, H. Liu, H. Bian, X. Meng, C. Shan, J. Si, Y. Zhao, X. Hou, Opt. Lett. **37**, 3825–3827 (2012).
[15] D. Wu, J. Xu, L.-G. Niu, S.-Z. Wu, K. Midorikawa, K. Sugioka, Light Sci. Appl. **4**, e228 (2015).
[16] A. Pan, B. Gao, T. Chen, J. Si, C. Li, F. Chen, X. Hou, Opt. Express **22**, 15245–15250 (2014).
[17] R. Osellame, H.J.W.M. Hoekstra, G. Cerullo, M. Pollnau, Laser Photon. Rev. **5**, 442–463 (2011).
[18] K. Sugioka, Y. Hanada, K. Midorikawa, Laser Photonics Rev. **4**, 386–400 (2010).
[19] P. Nagpal, N.C. Lindquist, S.-H. Oh, D.J. Norris, Science **325**, 594–597 (2009).
[20] M. J. Burek, Y. Chu, M. S. Z. Liddy, P. Patel, J. Rochman, S. Meesala, W. Hong, Q. Quan, M. D. Lukin, M. Lončar, Nature Commun. **5**, 5718 (2014).
[21] P. Rath, S. Khasminskaya, C. Nebel, C. Wild, W. H. P. Pernice, Nature Commun. **4**, 1690 (2013).
[22] L. Ji, Y.-F. Chang, B. Fowler, Y.-C. Chen, T.-M. Tsai, K.-C. Chang, M.-C. Chen, T.-C. Chang, S. M. Sze, E. T. Yu, J. C. Lee, Nano Lett. **14**, 813–818 (2014).
[23] Y. Lu A. Lal, Nano Lett. **10**, 4651–4656 (2010).
[24] A. Kiani, K. Venkatakrishnan, B. Tan, V. Venkataramanan, Opt. Express **19**, 10834–10842 (2011).
[25] M. Hermersdorf, C. Hibert, D. Grogg, A. M. Ionescu, Microelectron. Eng. **88**, 2556–2558 (2011).
[26] M. J. Smith, M.-J. Sher, B. Franta, Y.-T. Lin, E. Mazur, S. Gradečak, J. Appl. Phys. **112**, 083518 (2012).
[27] G. Molar-Velázquez, F. J. Renero-Carrillo, W. Calleja-Arriaga, Optik **121**, 843–846 (2010).
[28] Y. M. Sabry, B. Saadany, D. Khalil, T. Bourouina, Light Sci. Appl. **2**, e94 (2013).
[29] F. Merenda, M. Grossenbacher, S. Jeney, L. Forró, R.-P. Salathé, Opt. Lett. **34**, 1063–1065 (2009).
[30] Y.-K. Ee, P. Kumnorkaew, R. A. Arif, H. Tong, J. F. Gilchrist, N. Tansu, Opt. Express **17**, 13747–13757 (2009).

